THE JOURNAL OF PHYSICAL CHEMISTRY B

Article

pubs.acs.org/JPCB

Phase Behavior of Amphiphilic Diblock Co-oligomers with Nonionic and Ionic Hydrophilic Groups

Jennifer M. Heinen,[†,‡] Annabelle C. M. Blom,[†] Brian S. Hawkett,[†] and Gregory G. Warr*[,†]

[†]School of Chemistry, F11, The University of Sydney, NSW 2006, Australia

[‡]Department of Chemical and Biological Engineering, 2033 Sweeney Hall, Iowa State University, Ames, Iowa 50011, United States

Supporting Information

ABSTRACT: The synthesis of a series of co-oligomer amphiphiles by RAFT and their self-assembly behavior in water is described. These novel amphiphiles, comprised of styrene, butyl acrylate, and alkyl hydrophobes together with ionic acrylic acid and nonionic hydroxyethylacrylate hydrophilic moieties and with a total degree of polymerization from 5 to 17, represent a new class of small-molecule surfactants that can be formed from the immense potential library of all polymerizable monomers. Examples of micellar solutions and discrete cubic, hexagonal, lamellar, and inverted hexagonal lyotropic phases, as well as vesicle dispersions and coexisting lamellar phases, are reported and characterized by small-angle scattering. The variation of self-assembly structure with co-oligomer composition, concentration, and solution conditions is interpreted by analogy with the surfactant packing parameter used for conventional small-molecule amphiphiles.

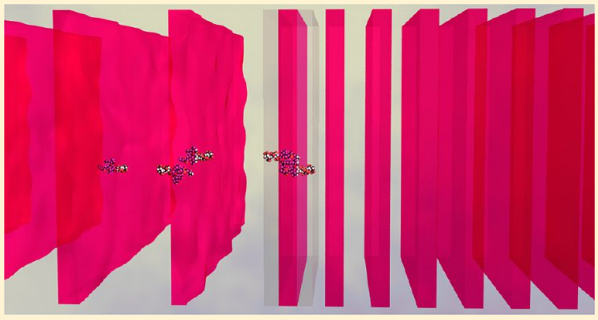

INTRODUCTION

Surfactants are amphiphilic molecules traditionally consisting of a nonionic or ionic hydrophilic headgroup and a hydrophobic alkyl tail. Surfactants are known to self-assemble in aqueous solution to form a range of microstructures from spherical micelles to hexagonally packed cylinders, bicontinuous cubic phases, and lamellar bilayers, in order of decreasing interfacial curvature.[1] The thermodynamically favorable self-assembled nanostructure of a surfactant in aqueous solution is a function of repulsive headgroup interactions, attractive hydrophobic tail interactions, and interfacial energy. Israelachvili et al. have developed a packing parameter model based on these interactions that relates the thermodynamically favorable self-assembled nanostructure to the molecular geometry of the surfactant in aqueous solution.[2] The model calculates the packing parameter (s) as the ratio of the molecular volume of the hydrophobic tail (v) to the product of the area of the headgroup at the interface (a_o) and the length of the hydrophobic tail (l), so $s = v/a_o l$. In other words, for $s = 1$, the molecule is cylindrical and preferentially packs into planar nanostructures, whereas for $s < 1$ the molecule is conical and preferentially packs into highly curved nanostructures, such as spheres or cylinders. Experimentally, the thermodynamically favorable self-assembled nanostructure of a particular surfactant in aqueous solution is a function of surfactant concentration and temperature.

The advent of controlled free radical polymerization techniques, such as reversible addition−fragmentation chain transfer (RAFT) polymerization[3] and atom transfer radical polymerization (ATRP),[4] has allowed for the facile synthesis of amphiphilic diblock copolymers with a broad range of chemical functionalities,[5−7] which may be used as novel amphiphiles. Diblock copolymers consist of two chemically distinct homopolymers that are covalently bound, so two incompatible blocks are unable to macrophase separate, and instead separate into ordered microdomains in bulk, aqueous solution, and mixed solvent systems, similar to traditional surfactants.[8−11] Amphiphilic diblock copolymers are an attractive alternative to traditional surfactants because they offer more variety in chemical composition, and molecular architecture. However, the prediction of thermodynamically favorable self-assembled nanostructures is more complex for diblock copolymers than traditional surfactants because the geometry of each block depends not only on the interfacial energy and intermolecular repulsive headgroup and attractive tail interactions but also on intramolecular interactions, such as core−chain stretching and corona−chain repulsions. The self-assembly of high molecular weight, amphiphilic block copolymers in aqueous solutions at low concentrations has been widely studied, and is described in several reviews of experimental[12−16] and theoretical[17] work. In particular, the review by Choucair and Eisenberg describes the strong effect of solution conditions, such as solvent, pH, and the concentration of additives including ions, surfactants, and homopolymers, on the intramolecular interactions of diblock copolymers.[18] Monte Carlo simulations of dilute diblock copolymers in selective solvents have also been used to improve

Received: August 8, 2012
Revised: February 17, 2013
Published: February 19, 2013

dx.doi.org/10.1021/jp307875z | J. Phys. Chem. B 2013, 117, 3005−3018

understanding of the underlying thermodynamics of diblock copolymer self-assembly. For example, Termonia has used Monte Carlo simulations of AB diblock copolymers in a selective solvent for the B block to predict the transition from spherical to cylindrical micelles, and related this to the packing parameter of Israelachvili et al.[2,19] These simulations showed that the relative interfacial area of each block, described as the square of the ratio of the radius of gyration of the hydrophobic block (A) to the hydrophilic block (B) ($[R_{g,A}/R_{g,B}]^2$), directly corresponds to the packing parameter, and predicts a transition from spheres to cylinders at a value of 0.5. Panagiotopoulous et al. have also used Monte Carlo simulations to investigate the relative free energies of micellization and phase separation for low molecular weight copolymers with hydrophilic head (H) and hydrophobic tail (T) block lengths ranging from 1 to 16.[20] These simulations predict that all symmetric diblocks and asymmetric diblocks with longer hydrophilic head groups thermodynamically favor micelle formation as opposed to phase separation. Also, hydrophobic diblocks with compositions of H_2T_4, H_4T_8, H_4T_{16}, and H_8T_{16} favor micellization over phase separation. However, phase separation is predicted if the length of the hydrophobic tail relative to the hydrophilic headgroup is increased further.

This work examines the effect of diblock co-oligomer composition and concentration on self-assembled nanostructures in aqueous solutions for a series of oligomers with nonionic 2-hydroxyethyl acrylate (HEA) and ionic acrylic acid (AA) hydrophilic head groups and butyl acrylate (BA) and styrene (S) hydrophobic tails. The effect of ionization of the AA headgroup on the self-assembled nanostructure is also investigated. The average total degree of polymerization for each co-oligomer is less than 15. In contrast to the vast number of studies on high molecular weight diblock copolymer self-assembly in dilute aqueous solutions, the self-assembly of low molecular weight, amphiphilic diblock co-oligomers over the entire concentration range in aqueous solutions has been largely unexplored. Recently, Siauw et al. examined the self-assembly of low molecular weight AA_{14}-b-$S_{y=16,33}$ and poly(ethylene glycol)$_{16}$-b-$S_{y=2,4,6}$ ($mPEG_{16}$-b-$S_{y=2,4,6}$) co-oligomers in aqueous solutions at a concentration of 6 mg of oligomer/mL.[21] They found that all of these co-oligomers form micelles at this low concentration, and that the diameter of the self-assembled micelles increases as the length of the hydrophobic block increases, as expected. Braun et al. have studied low molecular weight poly(ethylene oxide)$_{23}$-b-poly(γ-methyl-ε-caprolactone)$_{y=25,32,44,54}$ (PEO_{23}-b-$PMCL_{y=25,32,44,54}$) over the entire polymer concentration range in aqueous solutions.[22] These studies showed that the most prevalent self-assembled nanostructures for all of the diblock copolymer compositions are lamellar bilayers and vesicles. However, PEO_{23}-b-$PMCL_{25}$ also forms hexagonally packed cylinders at low polymer concentrations, and PEO_{23}-b-$PMCL_{54}$ forms inverse hexagonally packed cylinders at high polymer concentrations. These studies clearly demonstrate the effect of the hydrophobic block volume on the interfacial curvature of the self-assembled nanostructures.

Other previous studies of AA_x-b-S_y have focused on the formation of micelles in dilute aqueous solutions by the dissolution of high molecular weight diblock copolymer in a solvent that is good for both blocks, then addition of water, and subsequent dialysis to remove the original solvent.[23−27] This allows micelles to form under dynamic equilibrium. Several groups have conducted similar studies with AA_x-b-BA_y.[28−30] Cristobal et al. used small angle neutron scattering and dynamic light scattering to show that AA_{23}-b-BA_{167} and AA_{62}-b-BA_{111} form polydisperse core−shell micelles in aqueous solutions at polymer concentrations from 1 to 20 wt %, and that the AA blocks are significantly stretched.[29] Jacquin et al. studied AA_x-b-BA_y diblock copolymers with approximate total molecular weights of 10 000 g/mol in dilute aqueous solutions, and found that the self-assembled nanostructures were a function of the preparation method, which indicates that the structures did not reach thermodynamic equilibrium.[30]

Colombani et al. have also investigated the micellization of AA_x-b-BA_y at polymer compositions of AA_{100}-b-BA_{90}, AA_{150}-b-BA_{100}, and AA_{300}-b-BA_{90}, and found a slight increase in the aggregation number of the micelles as the degree of ionization of the AA decreases, consistent with a reduction in the headgroup size as electrostatic repulsion decreases. These studies have also shown that the kinetics of diblock copolymer exchange is slowed by the addition of salt, such that the observed micellar structure depends on the route of formation.[28]

Table 1 summarizes the diblock co-oligomers studied in this work. The radius of gyration of each block as a function of polymer composition and concentration is not known a priori, so no predictions of the self-assembled nanostructures based on a direct comparison to the work of Termonia and Israelachvili can be made.[2,19] Instead, Table 1 provides the ratio of the molecular volume of the hydrophobic block to the hydrophilic block, calculated from the known density and molecular weight of each

Table 1. Summary of Oligomers Studied, Showing Hydrophobic:Hydrophilic Block Molecular Volume Ratio Calculated from Monomer Densities and Molecular Weights

oligomer	hydrophobic/hydrophilic block volume ratio
HEA_5-C_{12}RAFT	0.28
HEA_8-C_{12}RAFT	0.18
HEA_{10}-C_{12}RAFT	0.15
HEA_5-b-BA_5-C_4RAFT	1.18
HEA_6-b-BA_5-C_4RAFT	1.00
HEA_7-b-BA_5-C_4RAFT	0.87
HEA_8-b-BA_5-C_4RAFT	0.77
AA_5-b-BA_5-C_4RAFT	
acidic	1.85
partially ionized	1.59
fully ionized	1.43
AA_5-b-BA_9-C_4RAFT	
acidic	3.23
partially ionized	2.78
fully ionized	2.50
AA_5-b-BA_{12}-C_4RAFT	
acidic	4.35
partially ionized	3.70
fully ionized	3.33
AA_5-b-S_5-C_4RAFT	
acidic	1.56
partially ionized	1.35
fully ionized	1.20
AA_5-b-S_9-C_4RAFT	
acidic	2.70
partially ionized	2.33
fully ionized	2.08
AA_5-b-S_{12}-C_4RAFT	
acidic	3.57
partially ionized	3.03
fully ionized	2.70

dx.doi.org/10.1021/jp307875z | J. Phys. Chem. B 2013, 117, 3005−3018

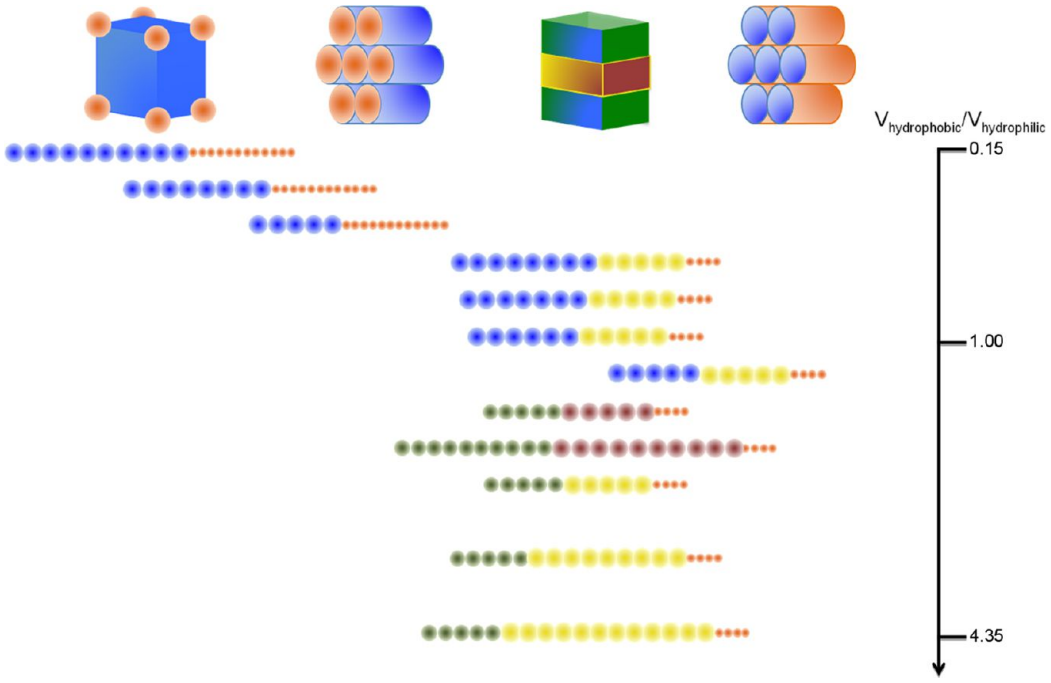

Figure 1. Summary of lyoptropic liquid crystal structure(s) formed by various diblock co-oligomers in concentrated aqueous solutions. AA_5-STY_{12}-C_4RAFT and AA_5-STY_9-C_4RAFT samples formed no structures (see text). Blue circles = HEA, green circles = AA (50% ionized), yellow circles = BA, red circles = STY, orange circles = CH_2.

monomer. At volume ratios significantly less than 1, the interfacial curvature of the thermodynamically favorable self-assembled nanostructure is predicted to be high to accommodate the packing constraints of the large hydrophilic headgroup and the short hydrophobic tails. As the ratio increases, first planar structures with zero mean interfacial curvature and then inverse nanostructures with negative interfacial curvature are anticipated. These predictions are most appropriate for the nonionic systems, as electrostatic repulsions between ionic head groups alter the effective headgroup area as a function of degree of ionization, co-oligomer composition, and concentration. Figure 1 summarizes the structures formed by the diblock co-oligomers in concentrated aqueous solutions relative to the molecular volume ratio of the hydrophobic to the hydrophilic block.

MATERIALS AND METHODS

Oligomer Synthesis. Oligomers were synthesized by reversible addition−fragmentation chain transfer (RAFT) polymerization using either the chain transfer agent 2-(((butylthio)carbonothioyl)thio)propanoic acid (C_4RAFT) or 2-(((dodecylthio)carbonothioyl)thio)propanoic acid (C_{12}RAFT), shown in Figure 2. These chain transfer agents differ only in the length of the alkyl chain that constitutes the hydrophobic Z group. The chain transfer agent was provided by Dulux Australia and used as received. 2-Hydroxyethyl acrylate (HEA, Aldrich), sodium hydroxide (NaOH, Aldrich), 1,4-dioxane (Fluka), and 4,4′-azobis(4-cyanopentanoic acid) (V501, Wako) were used as received. *n*-Butyl acrylate (BA, Aldrich) and styrene (S, Synthetic Resins) were purified by passage through a column packed with quaternary ammonium anion-exchange resin (Aldrich). Acrylic acid (AA, Sumika) was purified by distillation under reduced pressure. 2,2′-Azobisisobutyronitrile (AIBN, Fluka) was purified by recrystallization in ethanol.

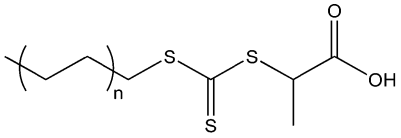

2-(((**alkyl**thio)carbonothioyl)thio)propanoic acid
C_4RAFT: n = 1, **alkyl** = butyl
C_{12}RAFT: n = 5, **alkyl** = dodecyl

Figure 2. Chain transfer agents used for oligomer synthesis.

A typical polymerization was performed as follows with the reaction conditions provided in Table 2. Table 1 summarizes all of the oligomers that were synthesized. The first monomer and the chain transfer agent were dissolved in dioxane in a round-bottom flask with a magnetic stirring bar at a molar ratio of monomer to chain transfer agent equal to the desired number of monomer repeat units per oligomer. Initiator was added to the dioxane solution at a concentration of 2 wt % relative to monomer. The round-bottom flask was sealed with a rubber septum, and the solution was purged with 99.999% nitrogen for 10 min. The round-bottom flask was then placed in an oil bath at elevated temperature with continuous mixing provided by the magnetic stirring bar. At the end of the first reaction time, the round-bottom flask was removed from the oil bath, and a small aliquot of the solution was removed for gravimetric analysis to calculate monomer conversion, and electrospray ionization mass spectroscopy (ESI-MS) to determine oligomer molecular weight. The second monomer was then added to the round-bottom flask at a molar ratio relative to the initial chain transfer agent concentration equal to the desired number of monomer repeat units per oligomer. The round-bottom flask was then sealed with a rubber septum, purged with 99.999% nitrogen for 10 min, and placed in an oil bath at elevated temperature with continuous mixing provided by the magnetic stirring bar. At the conclusion of the reaction time, a small aliquot of the solution

dx.doi.org/10.1021/jp307875z | *J. Phys. Chem. B* 2013, 117, 3005−3018

Table 2. Reaction Conditions for Each Type of Oligomer Synthesized as Described in the Text

polymer	1st monomer	2nd monomer	initiator	reaction T (°C)	1st reaction time (h)	2nd reaction time (h)
HEA_x-C_{12}RAFT	HEA		AIBN	70	3	
HEA_x-b-BA_5-C_4RAFT	HEA	BA	AIBN	70	3	12
AA_5-b-BA_y-C_4RAFT	AA	BA	V501	60	2	3
AA_5-b-S_y-C_4RAFT	AA	S	V501	60	2	9

was removed for gravimetric analysis, and ESI-MS. Then, the dioxane was removed by rotary evaporation under reduced pressure. Neutralized and half-neutralized AA oligomers were prepared by dissolving the dry oligomer in an aqueous 1.0 M NaOH solution at a molar ratio of NaOH to AA monomer units of 1:1 or 1:2, respectively.

Electrospray Ionization Mass Spectroscopy. The degree of polymerization of each oligomer block was determined by electrospray ionization mass spectroscopy (ESI-MS) using a Finnigan LCQ Mass Spectrometer. Aliquots of oligomer in dioxane removed at the conclusion of each polymerization were diluted 100 times in methanol, and 100 μL of sample was injected into the mass spectrometer. Standard Xcalibur software was used to monitor the elution of each positively charged species, and plot the relative abundance as a function of the mass per charge ratio (m/z).

Phase Study Sample Preparation. Samples of diblock co-oligomer in water were prepared at several concentrations ranging from 0.5 to 80 wt % polymer. Dry co-oligomer was weighed into a borosilicate glass sample vial, and Milli-Q deionized water was added to the desired concentration. The vials were sealed with a screw cap and Parafilm, and placed on a roller-mixer for 1 day. Samples were then placed in a water bath at 80 °C for 1 day, and mixed on the roller-mixer at room temperature for an additional 4 days before being allowed to equilibrate in a water bath thermostatted at 25 °C for several weeks prior to examination by polarizing optical microscopy or small-angle X-ray scattering (SAXS). Samples were checked daily, and the number of phases and visual appearance and birefringence of each phase were recorded. Samples were considered to have reached thermodynamic equilibrium when the observed phases remained unchanged for several days; however, it is probable that some samples remained kinetically trapped in a metastable state due to the slow rearrangement times of the co-oligomers.

Polarizing Optical Microscopy. Solvent penetration (flooding) experiments were used to identify the liquid crystal phases formed by each diblock co-oligomer. A small amount of co-oligomer was deposited onto a glass slide, covered by a coverslip, and gently pressed into a thin layer by applying pressure to the coverslip. The sample was then placed on the stage of a Leica DM2500P optical microscope equipped with a CCD camera, and viewed between crossed polarizers. The position of the stage was adjusted to focus on the edge of the polymer film, and a small drop of water was introduced at the edge of the coverslip. Capillary action drew the water under the coverslip to wet the sample, and produce a concentration gradient from pure water at the edge of the coverslip to pure co-oligomer at the center. The phases formed by the co-oligomer in aqueous solution appear in bands radiating from the center of the co-oligomer film. Anisotropic liquid crystal phases display characteristic textures when viewed between crossed polarizers, and isotropic liquid crystal phases appear transparent.[31−35] Equilibrated samples of co-oligomer in water were also examined with the polarizing optical microscope to identify the liquid crystal nanostructure from the characteristic textures observed.

Small Angle X-ray Scattering. Small angle X-ray scattering (SAXS) experiments were performed using an Anton Paar SAXSess at the University of Sydney and a Bruker Nanostar at the Bragg Institute at the Australian Nuclear Science and Technology Organisation (ANSTO). The Anton Paar SAXSess is equipped with a sealed tube source and three-pinhole collimation. The scattering intensity was collected on image plates, which were read with a Perkin-Elmer Cyclone phosphor storage system using standard OptiQuant software. The 2D intensity profiles were integrated using SAXSquant 2D software to produce plots of the intensity $(I(q))$ vs the scatting vector $(q = (4\pi/\lambda)\sin(\theta/2))$. The Bruker Nanostar has a rotating anode source (Cu Kα, 1.541 Å), three-pinhole collimation, cross-coupled Göbel mirrors, and a Hi-Star 2D detector with 100 μm resolution. Low viscosity samples were injected into a 2 mm diameter quartz capillary with 0.1 mm wall thickness. High viscosity samples were loaded into a paste cell with clear, amorphous poly(methyl methacrylate) windows. The sample cell was placed in the sample chamber, which was thermostatted at 25 °C, and the sample chamber and camera environment were evacuated prior to measuring the scattering intensity for 1 h. The scattering intensity, $I(q)$, was measured for equilibrated samples of co-oligomer in water at several concentrations. Liquid crystal phases were identified by the relative locations of the Bragg intensity peaks.[32] For example, the scattering from a lamellar nanostructure has intensity peaks at scattering vectors with a ratio of 1:2:3, whereas the ratio for hexagonally packed cylinders is $1:\sqrt{3}:\sqrt{4}$.

Small Angle Neutron Scattering. Small angle neutron scattering (SANS) measurements were performed on the NG7 beamline at the National Institute of Standards and Technology (NIST) Center for Neutron Research (NCNR). Three sample-to-detector distances from 1535 to 105 cm, corresponding to a scattering vector (q) range of 0.0015 and 0.230 Å^{-1}, were used to measure the scattered intensity. Equilibrated samples of co-oligomer in deuterium oxide (D_2O) were measured at 25 °C. Data were reduced and analyzed using SANS reduction and analysis packages for IGOR Pro, as provided by the NCNR.[36]

RESULTS

Degree of Polymerization and Molar Mass Dispersity. Polymeric amphiphiles differ from traditional surfactants due to their inherent dispersity in both molecular size (degree of polymerization) and composition. On the basis of the Gibbs phase rule, increasing dispersity theoretically increases the number of potential phases that may coexist at a given temperature and pressure because it effectively increases the number of components in the system. Although this effect of dispersity is rarely encountered in the high molecular weight, amphiphilic copolymer literature, knowledge of the degree of polymerization distribution and the composition distribution remains essential in analyzing the phase behavior of these molecules. Examples of the ESI-MS results for HEA_8-C_4RAFT

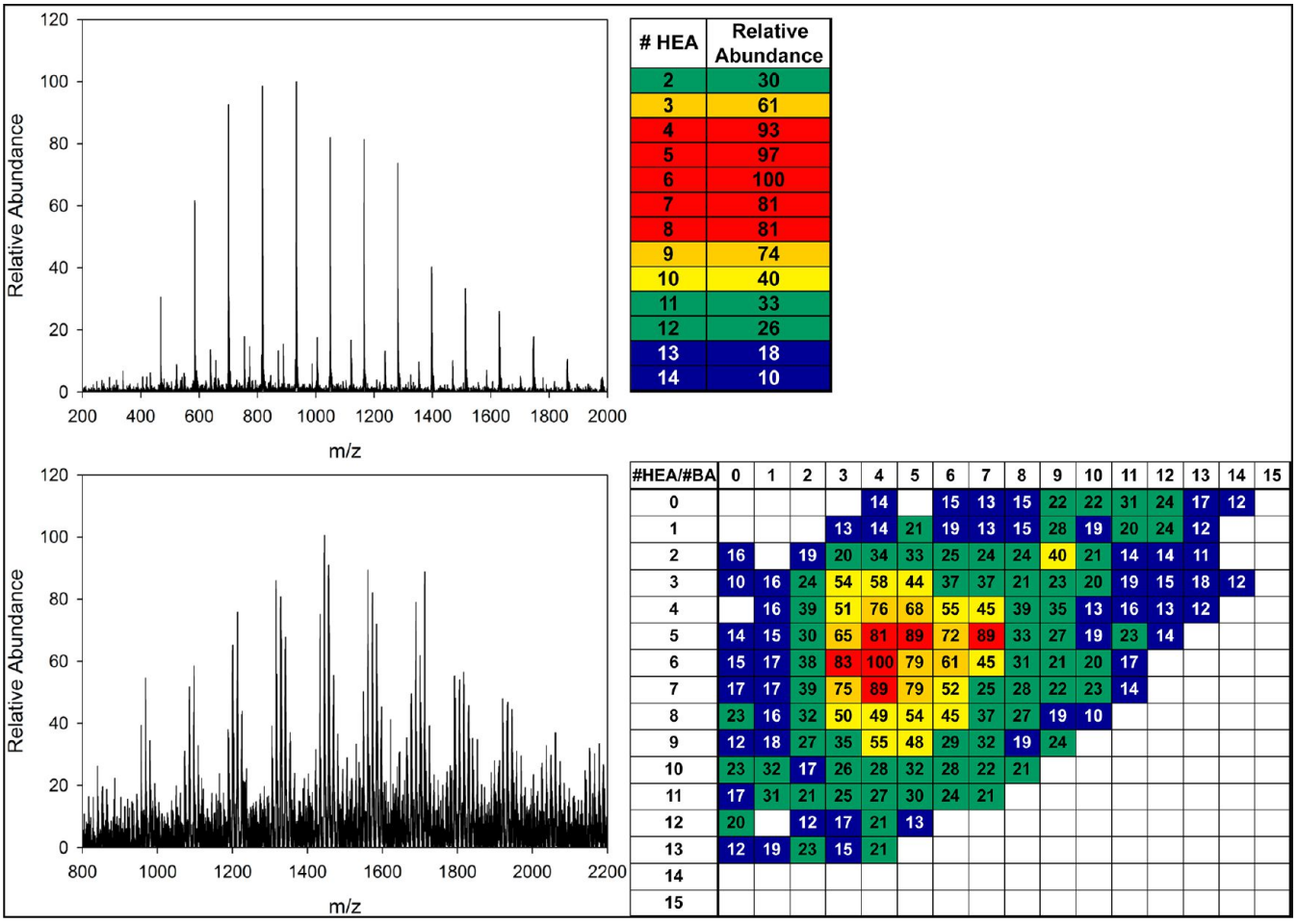

# HEA	Relative Abundance
2	30
3	61
4	93
5	97
6	100
7	81
8	81
9	74
10	40
11	33
12	26
13	18
14	10

#HEA/#BA	0	1	2	3	4	5	6	7	8	9	10	11	12	13	14	15
0					14		15	13	15	22	22	31	24	17	12	
1				13	14	21	19	13	15	28	19	20	24	12		
2	16		19	20	34	33	25	24	24	40	21	14	14	11		
3	10	16	24	54	58	44	37	37	21	23	20	19	15	18	12	
4		16	39	51	76	68	55	45	39	35	13	16	13	12		
5	14	15	30	65	81	89	72	89	33	27	19	23	14			
6	15	17	38	83	100	79	61	45	31	21	20	17				
7	17	17	39	75	89	79	52	25	28	22	23	14				
8	23	16	32	50	49	54	45	37	27	19	10					
9	12	18	27	35	55	48	29	32	19	24						
10	23	32	17	26	28	32	28	22	21							
11	17	31	21	25	27	30	24	21								
12	20		12	17	21	13										
13	12	19	23	15	21											
14																
15																

Figure 3. Electrospray ionization mass spectroscopy of HEA_8-C_4RAFT (top) and HEA_8-b-BA_5-C_4RAFT (bottom), and the relative abundance of each oligomer species scaled such that 100 represents the most abundant species. Only species with a relative abundance greater than 10 are shown.

homo-oligomer and the subsequent HEA_8-b-BA_5-C_4RAFT co-oligomer are shown in Figure 3. The primary peaks observed in the ESI-MS spectrum for HEA_8 correspond to polymer with an R group from the chain transfer agent at one end and the S—C(Z)═S group from the chain transfer agent at the other end. These oligomers are dormant, and may be reinitiated in subsequent polymerizations. Terminated oligomers with an R group at one end and a saturated C—C bond at the other end are also evident in the ESI-MS spectrum although in much lower abundance. These oligomers cannot be reinitiated in subsequent polymerizations, so the diblock co-oligomer samples also contain a small amount of HEA homo-oligomer.

The ESI-MS spectrum of HEA_8-C_4RAFT shows that the homo-oligomer consists of a distribution of HEA_x with x ranging from 2 to 14 monomer units. The greatest proportion of the oligomers has 6 HEA monomer units. Each of the dormant chains from this polymerization may be reactivated during the polymerization of BA to form HEA_x-b-BA_y-C_4RAFT co-oligomer, thus further increasing the breadth of the molecular weight and composition distributions. The ESI-MS spectrum of HEA_8-b-BA_5-C_4RAFT shows a broad distribution with a maximum at HEA_6-b-BA_4-C_4RAFT. A low relative abundance of both HEA and BA homo-oligomers is also evident from the ESI-MS spectrum. All of the oligomers synthesized have a similar degree of dispersity in degree of polymerization and composition.

Phase Behavior of Nonionic Amphiphilic Oligomers. *HEA_x-C_{12}RAFT.* Hydroxyethyl acrylate homo-oligomers with three different degrees of polymerization were synthesized via RAFT polymerization using a chain transfer agent with a 12-carbon hydrophobic Z-group (Figure 2), namely, HEA_5-C_{12}RAFT, HEA_8-C_{12}RAFT, and HEA_{10}-C_{12}RAFT. On the basis of the relative molecular volumes of the hydrophobic and hydrophilic blocks (Table 1), all three of these oligomers are expected to self-assemble into normal nanostructures with the hydrophobic C_{12}RAFT on the inside, and high interfacial curvature to accommodate the geometric packing constraints of the relatively bulky hydrophilic headgroup and short hydrophobic tail. Interfacial curvature is expected to increase as the HEA block length increases from 5 to 8 to 10.

Solvent penetration (flooding) experiments reveal the optical texture of a hexagonally packed cylinder nanostructure at high concentrations of HEA_5-C_{12}RAFT in aqueous solution, whereas the HEA_8-C_{12}RAFT and HEA_{10}-C_{12}RAFT oligomers show no anisotropic phases at any concentration. The SAXS spectra of HEA_5-C_{12}RAFT (Figure 4a) confirm that a hexagonally packed cylinder nanostructure with a peak ratio of $1:\sqrt{3}:\sqrt{4}$ exists at 79.4 wt % oligomer in water. Visual inspection of samples between crossed polarizers indicates that samples are biphasic between 43.5 and 69.4 wt % HEA_5-C_{12}RAFT with a lower birefringent phase and an upper isotropic phase, which indicates coexistence of isotropic micellar and anisotropic hexagonally packed cylinder nanostructures. SAXS spectra show a weakly

dx.doi.org/10.1021/jp307875z | J. Phys. Chem. B 2013, 117, 3005−3018

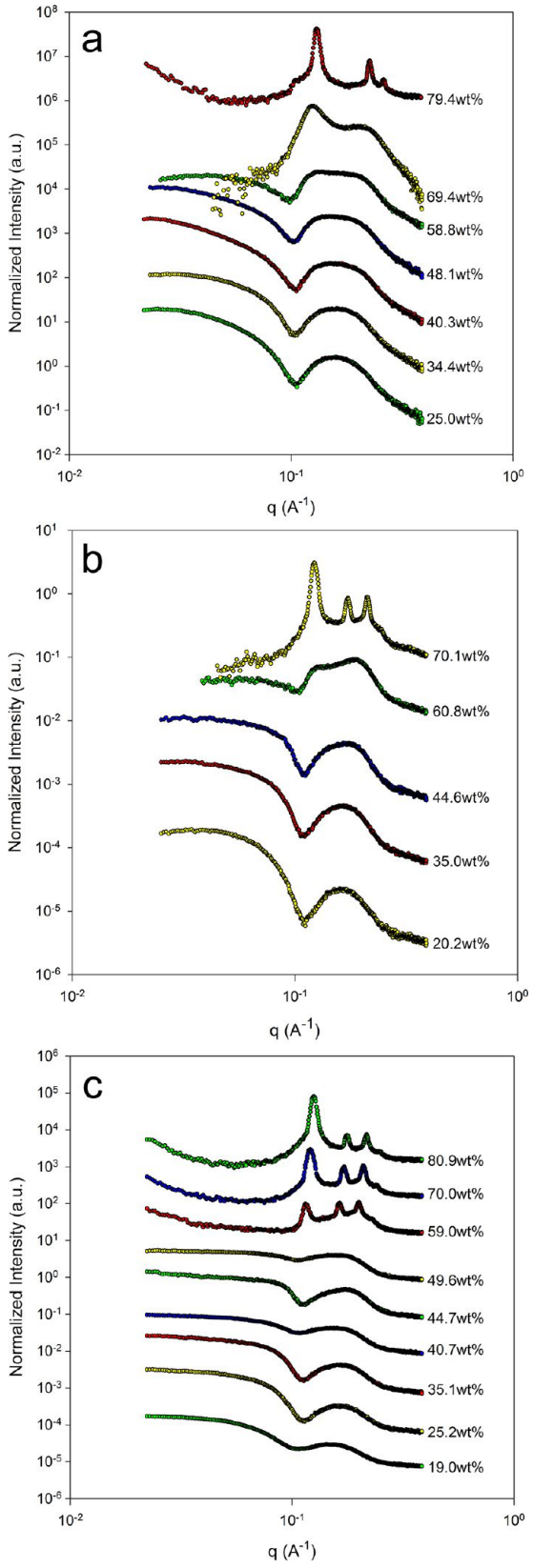

Figure 4. SAXS spectra of (a) HEA_5-C_{12}RAFT, (b) HEA_8-C_{12}RAFT, and (c) HEA_{10}-C_{12}RAFT in aqueous solution. Traces have been offset for clarity.

segregated nanostructure in the biphasic 58.8 wt % HEA_5-C_{12}RAFT sample and more apparent nanostructure in the 69.4 wt % HEA_5-C_{12}RAFT sample. However, the peaks are broad and the relative locations of the peak maxima do not correspond to any common liquid crystal structures. These diffuse peaks may indicate slow rearrangement of the oligomers into a hexagonally packed cylinder nanostructure.

The single phase 25 wt % HEA_5-C_{12}RAFT SAXS data has been fit to a polydisperse core-three shell spherical model with a pure hydrocarbon core, a S—C═S inner shell from the chain transfer agent, a pure HEA middle shell, and an outer shell of HEA swollen with water.[36,37] Models with less than three shells, and a prolate ellipsoid model were unable to fit the scattering at high q, as shown in the Supporting Information. The best fit of the data to the core-three shell model gives a core radius of 3 Å with a polydispersity, defined as the standard deviation divided by the core radius, equal to 1. The core radius is significantly less than the fully extended C_{12} alkyl chain length (19 Å), indicating that the hydrophobic tails are highly entangled within the core of the micelle. The thickness of the S—C═S shell is 9 Å, which is over twice the S—C═S bond length of 3.5 Å, and indicates that this shell is not well ordered. The pure HEA shell thickness of 17 Å and the outer HEA/water shell thickness of 9 Å give a total hydrophilic shell thickness of 26 Å, which is greater than the fully extended HEA_5 chain length (15.4 Å), However, this hydrophilic shell thickness agrees well with the average HEA_{4-13} chain length of 25.3 Å calculated from a weighted average based on the ESI-MS molar mass distribution.

The HEA_8-C_{12}RAFT and HEA_{10}-C_{12}RAFT SAXS spectra (Figure 4b and c) display a strongly segregated *Im*3*m* cubic phase with a peak spacing of $\sqrt{2}$:$\sqrt{4}$:$\sqrt{6}$:$\sqrt{8}$ at high concentrations. This is consistent with the lack of detectable birefringence at any concentration. The emergence of this discrete cubic phase is also consistent with the greater molecular volume of the hydrophilic block in HEA_8-C_{12}RAFT and HEA_{10}-C_{12}RAFT relative to HEA_5-C_{12}RAFT favoring a nanostructure with higher interfacial curvature than hexagonally packed cylinders. Like HEA_5-C_{12}RAFT, HEA_{10}-C_{12}RAFT has a large biphasic region (from 30.3 to 49.6 wt % polymer), whereas HEA_8-C_{12}RAFT is a single phase over the entire concentration range examined.

HEA_x-b-BA_5-C_4RAFT. Changing the hydrophobe from -C_{12}RAFT to -BA_5-C_4RAFT significantly increases the volume of the hydrophobic block, which alters the geometric packing constraints to favor nanostructures with a more planar or inverse interfacial curvature (Table 1). Solvent penetration experiments and SAXS (Figure 5) both show that HEA_5-BA_5-C_4RAFT forms a lamellar phase at intermediate oligomer concentrations and an inverse hexagonal phase at high oligomer concentrations, whereas $HEA_{x=6-8}$-BA_5-C_4RAFT oligomers only form lamellar nanostructures, in accordance with the predicted trends in interfacial curvature (Table 1). HEA_5-BA_5-C_4RAFT is biphasic between 15 and 80 wt % in water. The top phase is isotropic, while the bottom phase is viscous and very weakly birefringent when viewed between crossed polarizers. Solvent penetration experiments show characteristic lamellar textures at intermediate oligomer concentrations; however, the characteristic Bragg peaks are not observed in the SAXS spectra (Figure 5a). The SAXS spectra do indicate ordered domains at polymer concentrations above 50.3 wt %, but very weak secondary and tertiary Bragg peaks with the 1:$\sqrt{3}$:$\sqrt{4}$ ratio corresponding to a hexagonally packed cylinder nanostructure can only be observed at 81.3 wt % HEA_5-b-BA_5-C_4RAFT (Figure 5a).

At high polymer concentrations, $HEA_{x=6-8}$-BA_5-C_4RAFT co-oligomers all self-assemble into lamellar nanostructures with Bragg peaks in the characteristic 1:2 ratio (Figure 5b–d).

dx.doi.org/10.1021/jp307875z | *J. Phys. Chem. B* 2013, 117, 3005–3018

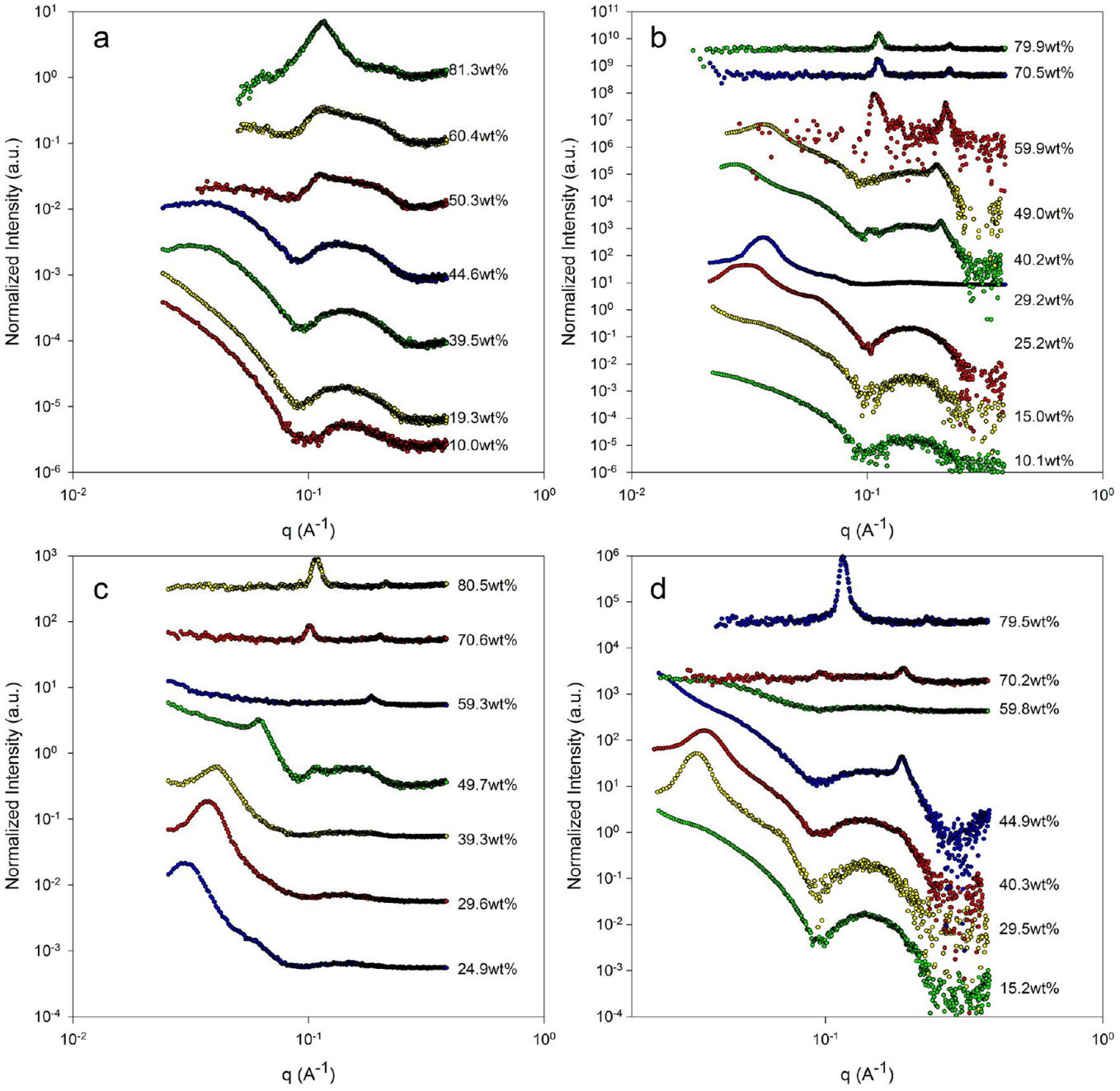

Figure 5. SAXS spectra of (a) HEA_5-b-BA_5-C_4RAFT, (b) HEA_6-b-BA_5-C_4RAFT, (c) HEA_7-b-BA_5-C_4RAFT, and (d) HEA_8-b-BA_5-C_4RAFT. Spectra are offset for clarity.

Polarizing optical microscopy indicates characteristic lamellar textures at all $HEA_{x=6-8}$-BA_5-C_4RAFT concentrations. HEA_6-BA_5-C_4RAFT SAXS spectra were well-described by fitting to a head−tail lamellar bilayer model using IGOR and an analysis package provided by the National Institute of Standards and Technology (NIST) Center for Neutron Research (NCNR).[36,38] This model calculates the scattered intensity $I(q)$ as

$$I(q) = \frac{2\pi P(q)S(q)}{dq^2}$$

where the form factor $P(q)$ is

$$P(q) = \frac{4}{q^2}[\Delta\rho_H(\sin[q(\delta_H + \delta_T)] - \sin[q\delta_T]) + \Delta\rho_T \sin(q\delta_T)]^2$$

and the structure factor $S(q)$ is

$$S(q) = 1 + 2\sum_1^{N-1}\left(1 - \frac{n}{N}\right)\cos\left(\frac{qdn}{1 + 2\Delta q^2 d^2 \alpha(n)}\right) \exp\left(-\frac{2q^2d^2\alpha(n) + \Delta q^2 d^2 n^2}{2(1 + 2\Delta q^2 d^2 \alpha(n))}\right)\frac{1}{\sqrt{2\Delta q^2 d^2 \alpha(n)}}$$

with the Caillé parameter

dx.doi.org/10.1021/jp307875z | J. Phys. Chem. B 2013, 117, 3005−3018

$$\eta_{CP} = \frac{{q_0}^2 k_B T}{8\pi\sqrt{K\bar{B}}}$$

and

$$\alpha(n) = \frac{\eta_{CP}}{4\pi^2}[\ln(\pi n) + \gamma_E] \quad \text{with} \quad \gamma_E \approx 0.577$$

The parameters in this model are the repeat spacing (d), the headgroup and tail thickness (δ_H and δ_T), the differences in scattering length density (SLD) between the headgroup and the solvent ($\Delta\rho_H = SLD_{head} - SLD_{H_2O}$) and between the tail and the headgroup ($\Delta\rho_T = SLD_{tail} - SLD_{head}$), the instrumental resolution (Δq), the smectic bending elasticity (K), the compression modulus ($\bar{B}$), and the number of lamellar plates (N).[36,38] The SLDs of the headgroup, the tail, and the solvent were calculated, and $\Delta\rho_H$ and $\Delta\rho_T$ were fixed. The model fitting routine is very sensitive to the initial values of the remaining parameters (d, δ_H, δ_T, η_{cp}), and these values must also be constrained to physically realistic values. The repeat spacing was constrained to 20 Å < d < 500 Å. The fully extended length of the HEA_6 headgroup, including the R group of the chain transfer agent, is approximately 21 Å, and the fully extended length of the BA_5-C_4RAFT tail is approximately 19 Å, so the thickness of the headgroup and the tails was constrained to 1 Å < δ_H and δ_T < 20 Å. The Caillé parameter was constrained to 0 < η_{cp} < 0.8, which is the valid range of values for this particular model.

Best-fit structural parameters are listed in Table 3. The tail thickness remains constant within experimental uncertainty at 8.4 ± 0.4 Å at all concentrations. This is less than half the fully extended length of BA_5-C_4RAFT (19 Å), suggesting that blocks on opposite sides of the bilayer are intercalated. The headgroup thickness agrees well with the calculated fully extended HEA_6 length (21 Å), indicating that the HEA is highly swollen with water. The headgroup thickness decreases as the oligomer concentration increases, consistent with reduced solvation of the HEA. The repeat spacing also decreases continuously throughout the dilute single-phase region from 433 Å at 10.1 wt % HEA_6-BA_5-C_4RAFT to 169 Å at 29.3 wt % HEA_6-BA_5-C_4RAFT, and the Caillé parameter decreases from 0.56 to 0.23 as the co-oligomer concentration increases in this dilute lamellar region. This is expected as the Helfrich undulation forces are damped by an increasing confinement of neighboring bilayers. Above 59.9 wt % oligomer, a single, concentrated lamellar phase exists with decreasing repeat spacing, and a much smaller Caillé parameter (0.00−0.03), which indicates that these bilayers are much more rigid and/or well-ordered. Here the repeat spacing of 56−58 Å is comparable to the overall bilayer thickness of 32 Å, equal to twice the sum of the head and tail lengths. At 40.2 and 49 wt % HEA_6-BA_5-C_4RAFT in water, the samples are biphasic, and the SAXS spectra were fit to a model of *two* coexisting lamellar phases. This reduces the accuracy of the best-fit parameters but clearly reveals two distinct bilayer repeat spacings (190 ± 25 and 62.3 ± 1.4 Å) that correspond to the bilayer spacings at the dilute and concentrated phase boundaries (170 and 58 Å). Fitting of the HEA_7-BA_5-C_4RAFT and HEA_8-BA_5-C_4RAFT SAXS data indicates a similar formation of two distinct lamellar phases; however, the data could not be fit to within an acceptable degree of error.

Table 3. Summary of Nanostructures Formed by HEA_6-BA_5-C_4RAFT as Determined by Best Fits of SAXS Data to the Head−Tail Lamellar Model Described in the Text

wt % HEA_6-BA_5-C_4RAFT	head group thickness (Å)	tail thickness (Å)	lamellar spacing (Å)	Caillé parameter
10.1	21	8	433	0.56
15	20	8	329	0.46
25.2	18	8	193	0.26
29.3	16	9	169	0.23
40.2	16	9	215	0.57
	14	8	61	0.02
49	16	9	165	0.58
	17	8	64	0.10
59.9	8	9	58	0.03
70.5	8	8	56	0.00
77.9	8	8	56	0.02

Coexistence of two distinct lamellar phases has been previously observed for ionic amphiphiles in aqueous solutions, and is attributed to the presence of two types of repulsive forces between the head groups. Usually, these are short-range hydration forces and long-range electrostatic or (Helfrich) fluctuation interactions.[39−41] Thus, the formation of two distinct lamellar phases for solutions of the nonionic $HEA_{x=6-8}$-BA_5-C_4RAFT diblock co-oligomers in solution is not entirely unexpected, and may have arisen through a number of mechanisms. The large difference in Caillé parameters for the dilute and concentrated lamellar phases is highly suggestive of an "unbinding" transition between condensed lamellae and highly fluctuating, entropically favored bilayers discussed by several authors,[42] and predicted to be first-order by Wennerström.[43] It is also possible that a charge is imparted to the HEA block by deprotonation of the carboxylic acid in the R group of the chain transfer agent, contributing an electrostatic component to the long-range repulsion. Demé et al. have also shown that the introduction of polymer that can anchor to dimyristoylphosphatidylcholine (DMPC) bilayers in aqueous solutions induces the formation of two distinct lamellar phases due to the introduction of an additional steric repulsion between the bilayers.[44] As all of the $HEA_{x=6-8}$-BA_5-C_4RAFT diblock co-oligomer samples contain a small amount of HEA homo-oligomer, this could also introduce an additional steric contribution to the headgroup interactions.

Phase Behavior of Ionic Amphiphiles. *AA_5-b-BA_y-C_4RAFT.* Ternary phase diagrams for AA_5-b-BA_5-C_4RAFT, AA_5-b-BA_9-C_4RAFT, and AA_5-b-BA_{12}-C_4RAFT as a function of ionization of the AA block, generated from a combination of polarizing optical microscopy and SAXS, are shown in Figure 6. The protonated (neutral) forms of AA_5-b-BA_y-C_4RAFT diblock co-oligomers were only sparingly soluble in water and did not form ordered nanostructures. However, when at least half of the acrylic acid groups were ionized by neutralization with NaOH, these co-oligomers self-assembled in aqueous solutions to form predominantly lamellar phases. As the BA block increases in length, the co-oligomer solubility in water decreases, and so does the concentration at which the lamellar nanostructures form. The concentration range over which a lamellar nanostructure is observed also decreases. Reducing the charge on the headgroup likewise reduces the solubility of the co-oligomer and hence the concentration at which each phase is observed. Dilution of the lamellar phases of AA_5-b-BA_9-C_4RAFT and AA_5-b-BA_{12}-C_4RAFT yields long-lived vesicle dispersions, but dilution of AA_5-b-BA_5-C_4RAFT induces rearrangement of the co-oligomers into micelles. The fully ionized Na^+ AA_5-b-BA_5-C_4RAFT has a very large micellar L_1 region that persists up to almost 50 wt % co-

dx.doi.org/10.1021/jp307875z | J. Phys. Chem. B 2013, 117, 3005−3018

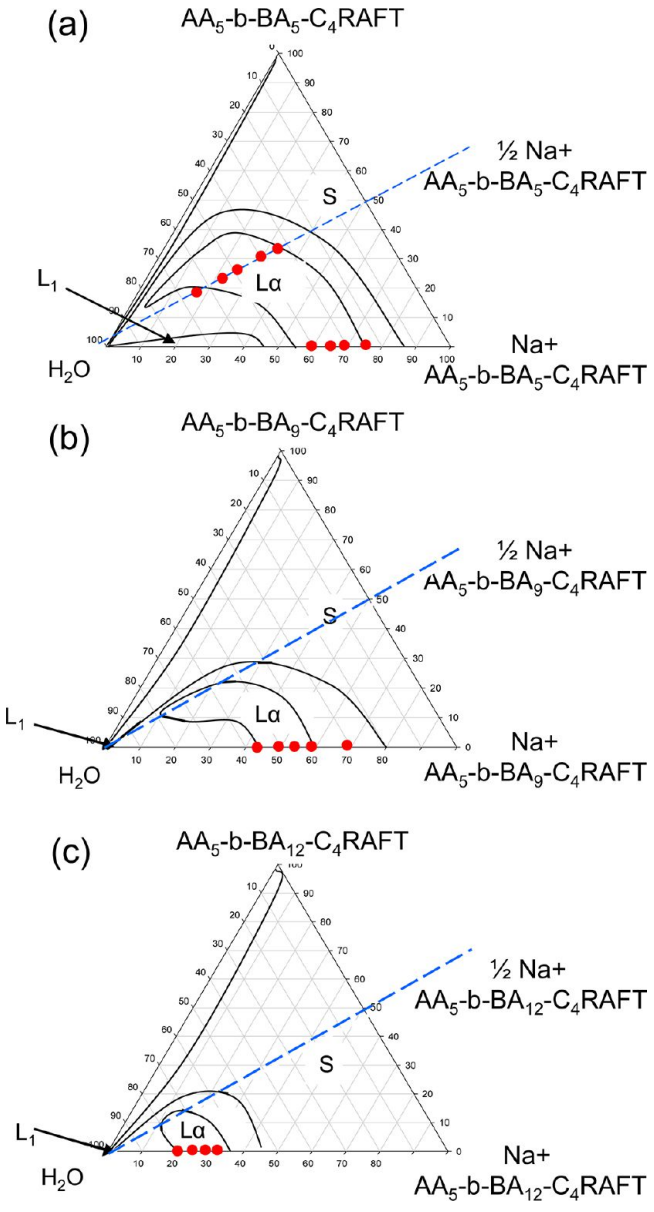

Figure 6. Ternary phase diagrams of (a) AA_5-b-BA_5-C_4RAFT, (b) AA_5-b-BA_9-C_4RAFT, and (c) AA_5-b-BA_{12}-C_4RAFT in water at 25 °C as a function of degree of ionization. The phase boundaries of the one-phase regions are drawn with a solid line. S, Lα, and L_1 denote solid, lamellar, and micellar phases. Concentrations are expressed in wt %. SAXS measurements were performed at concentrations marked by solid circles.

oligomer. All other AA_5-b-BA_y-C_4RAFT diblock co-oligomers form L_1 micellar phases only at very low concentrations, around 1 wt %.

SAXS spectra for Na^+ AA_5-b-BA_5-C_4RAFT, $^1/_2Na^+$ AA_5-b-BA_5-C_4RAFT, and Na^+ AA_5-b-BA_9-C_4RAFT samples in the lamellar phase are shown in Figure 7. These were fit to the same head−tail lamellar model used for HEA_6-BA_5-C_4RAFT, and the best-fit structural parameters are presented in Table 4. Some of the scattering curves, such as Na^+ AA_5-b-BA_9-C_4RAFT between 45 and 55 wt % (Figure 6c), show an intensity anomaly between the first and second order Bragg peaks. Similar features have been reported previously in X-ray and neutron scattering spectra from lamellar phases, and have been attributed to modulation of Bragg peak intensities by bilayer form factor effects.[38,45] All of these features were very well described by the head−tail lamellar model, shown in Figure 7 as solid lines.

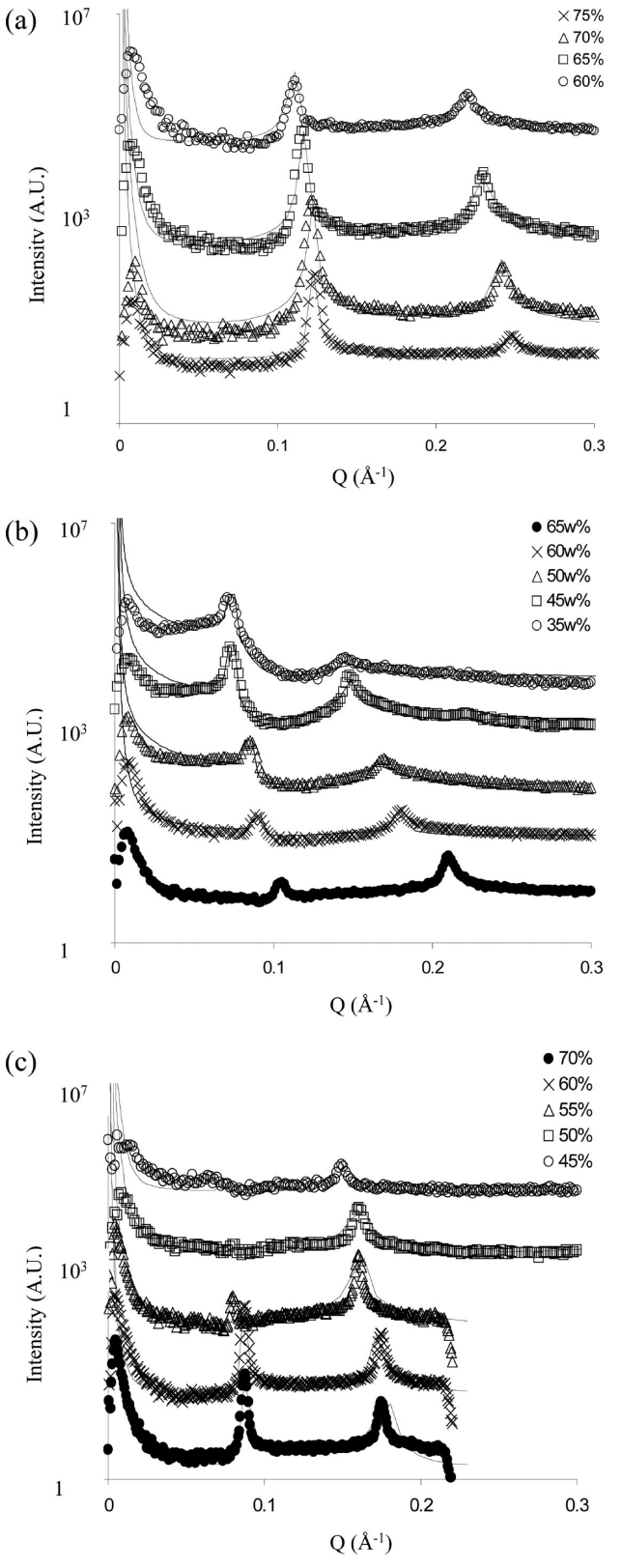

Figure 7. SAXS spectra of fitted (a) Na^+ AA_5-b-BA_5-C_4RAFT, (b) $^1/_2Na^+$ AA_5-b-BA_5-C_4RAFT, and (c) Na^+ AA_5-b-BA_9-C_4RAFT. Solid lines are fits to the head−tail lamellar model described in the text. Spectra have been offset by 10 for clarity.

dx.doi.org/10.1021/jp307875z | J. Phys. Chem. B 2013, 117, 3005−3018

Table 4. Summary of Lamellar Nanostructures Formed by Fully and Partially Ionized AA_x-b-BA_5-C_4RAFT from Best Fits to SAXS Data Using the Head−Tail Lamellar Model Described in the Text

	headgroup thickness (Å)	tail thickness (Å)	lamellar spacing (Å)	H_2O:AA_n	Caillé parameter
		Na^+ AA_5-b-BA_5-C_4RAFT			
75 wt %	11	7	51	46.1	0.09
70 wt %	8	7	52	38.5	0.14
65 wt %	9	6	55	52.4	0.15
60 wt %	8	6	57	44.0	0.19
		$^1/_2Na^+$ AA_5-b-BA_5-C_4RAFT			
65 wt %	7	6	61	36.0	0.12
60 wt %	8	10	70	14.1	0.15
50 wt %	10	12	74	15.6	0.25
45 wt %	10	14	85	10.5	0.20
35 wt %	10	14	86	10.5	0.35
		Na^+ AA_5-b-BA_9-C_4RAFT			
70 wt %	12	14	71	27.1	0.01
60 wt %	12	14	73	28.4	0.02
55 wt %	12	13	78	33.1	0.06
50 wt %	12	13	78	33.9	0.08
45 wt %	12	13	85	31.9	0.08

The tail thickness of the fully ionized Na^+ AA_5-b-BA_5-C_4RAFT lamellar bilayers is less than *half* of the extended length of 19 Å expected for a single BA_5-C_4RAFT block, and comparable to the corresponding tail thickness of the HEA bilayers (8.4 ± 0.4 Å). As in the case of the HEA_5-BA_y-C_4RAFT bilayers, this implies that the BA tails are intercalated with the tails of the opposing membrane. In contrast to the nonionic HEA head groups, the charged AA_5 chains are not fully extended but are only half of the fully extended AA block length. The AA layer does, however, contain a high proportion of water, which is consistent with strong repulsions between AA_5 chains. The effective molecular volume of AA_5 is thus much greater than its physical volume; thus, the Na^+ AA_5-b-BA_5-C_4RAFT diblock co-oligomers favor planar nanostructures rather than the inverted self-assembled nanostructures predicted (Table 1). The bilayer spacings and Caillé parameters are similar to the values calculated for the concentrated HEA_5-BA_6-C_4RAFT bilayers and indicated rigid, well-ordered structures.

Lowering the charge of AA_5-b-BA_5-C_4RAFT to 50% ionization or increasing the BA block length from five to nine yields broadly consistent behavior in the lamellar phase. The lamellar membranes are very thin, with the HEA head groups contracted and the BA tails intercalated with the tails of the opposing membrane. However, decreasing the ionization of the headgroup does cause a slight increase in membrane thickness and flexibility, as indicated by an increase in Caillé parameter. These structural changes, and the significant decrease in the H_2O:AA_5 chain ratio, are consistent with a reduction in nearest-neighbor headgroup repulsions. The increase in flexibility is also expected from a system that forms a vesicle dispersion when diluted.

SAXS spectra of Na^+ AA_5-b-BA_{12}-C_4RAFT are shown in Figure 8 together with a representative polarizing optical microscopy image indicative of a lamellar phase that forms a vesicle dispersion when diluted. The scattering displays relatively weak order compared to the AA_5-b-BA_y-C_4RAFT co-oligomers with shorter BA blocks (Figure 7), and the peak positions do not follow the expected 1:2:3 order, nor that of any other known lyotropic phase. Some features of the spectra were described

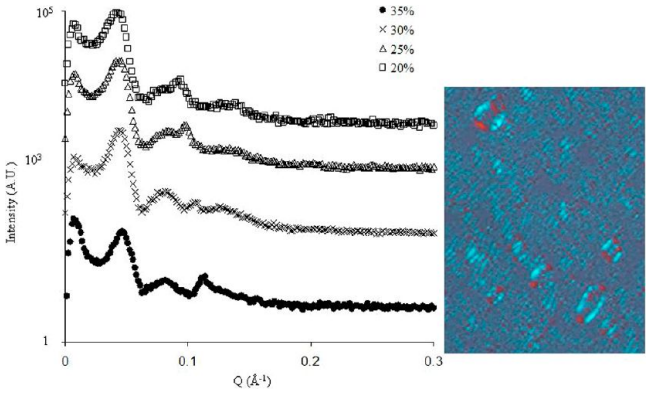

Figure 8. SAXS spectra of the Na^+ AA_5-b-BA_{12}-C_4RAFT lamellar phase as a function of dilution and polarizing optical micrograph of 35 wt % Na^+ AA_5-b-BA_{12}-C_4RAFT. Spectra have been offset by a factor of 10 for clarity.

moderately well using a stacked-disc model,[46] commonly used to describe the structure of organophilic clay platelets dispersed in organic solvents. This suggests a disordered but locally lamellar structure that does not anneal despite being heated, rolled, and left to equilibrate for many days prior to being examined. On the basis of previous studies of related diblock copolymer amphiphiles, this suggests that the BA_{12}-C_4RAFT hydrophobe is no longer sufficiently labile to equilibrate on the time scales expected of small amphiphiles.[47]

The self-assembled nanostructures of AA_5-b-BA_y-C_4RAFT co-oligomers in dilute solutions were probed using small angle neutron scattering (SANS) (Figure 9). The nanostructures

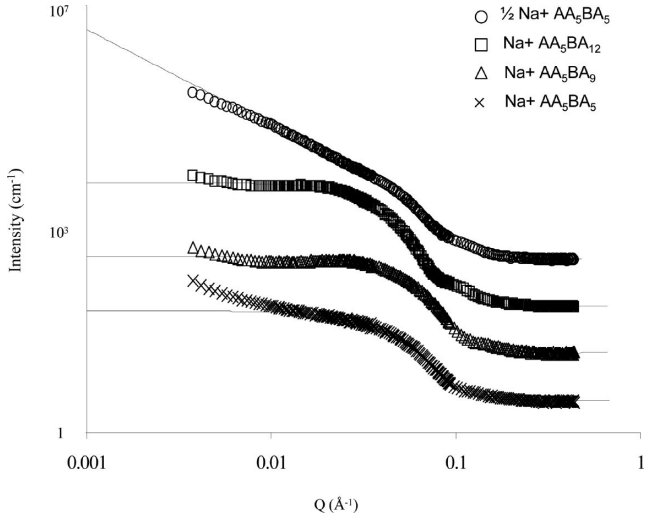

Figure 9. SANS spectra of 1 wt % $^1/_2Na^+$ AA_5-b-BA_5-C_4RAFT, Na^+ AA_5-b-BA_{12}-C_4RAFT, Na^+ AA_5-b-BA_9-C_4RAFT, and Na^+ AA_5-b-BA_5-C_4RAFT solutions in D_2O. Spectra have been offset by 10 for clarity.

differed sufficiently to require fitting to several models within the NIST Igor fitting package, including core−shell spheres, core−shell oblate ellipsoids, and dilute lamellar bilayers.[36,37,48,49] The results of the fitting are presented in Table 5. Fully ionized Na^+ AA_5-BA_5-C_4RAFT was best modeled by a (slightly polydisperse) core−shell sphere form factor. At 1 wt %, the BA_5-C_4RAFT core radius is less than its fully extended chain length of 19 Å, whereas the shell thickness indicates extended and strongly hydrated AA_5 chains, similar to the chain conformations in the lamellar bilayers

dx.doi.org/10.1021/jp307875z | J. Phys. Chem. B 2013, 117, 3005−3018

Table 5. Nanostructure of the Micelles Formed by AA_5-b-BA_y-C_4RAFT in D_2O as Measured by SANS and Determined from Best Fits to Models Described in the Text

	major core radius (Å)	minor core radius (Å)	shell thickness (Å)	aggregation number
8 wt % Na^+ AA_5-b-BA_5-C_4RAFT	18		10	21
1 wt % Na^+ AA_5-b-BA_5-C_4RAFT	13		19	7
1 wt % Na^+ AA_5-b-BA_9-C_4RAFT	41	25	8	103
1 wt % Na^+ AA_5-b-BA_{12}-C_4RAFT	62	39	9	228
1 wt % $^1/_2Na^+$ AA_5-b-BA_5-C_4RAFT	11	11	12	9

formed at high concentrations. The aggregation number at 1 wt %, based on core radius and bulk BA density, is only 7. At 8 wt % Na^+ AA_5-b-BA_5-C_4RAFT, the core radius is 18 Å, which corresponds to the fully extended length of a BA_5-C_4RAFT hydrophobic chain, and the aggregation number is 21. These trends are as expected for a traditional alkyl-tailed amphiphile.

In contrast, the SANS spectra of the longer tailed Na^+ AA_5-b-BA_9-C_4RAFT and Na^+ AA_5-b-BA_{12}-C_4RAFT could no longer be fit with a spherical core−shell model. Instead, a core−shell oblate ellipsoid form factor best fit the data. In 1 wt % solutions, best-fit minor core radii of 25 and 39 Å are consistent with fully extended hydrophobe lengths of 28 Å and 39 Å for BA_9-C_4RAFT and BA_{12}-C_4RAFT, respectively, and the axial ratios are approximately 1.5. Oblate micelles are unusual in conventional surfactant systems, which typically undergo a sphere-to-cylinder transition through a prolate ellipsoid intermediate. However, in these systems, a lamellar phase is the only liquid crystal phase observed, and the hydrophobic to hydrophilic block volume ratios are consistent with planar or even inverted structures. Therefore, an oblate or disk-like micelle is a reasonable expectation.

The SANS spectra for the partially ionized $^1/_2Na^+$ AA_5-b-BA_5-C_4RAFT display the characteristic low angle q^{-2} decay of a planar structure and were best-fit to a bilayer form factor. The hydrophobic thickness of 11 Å is in excellent agreement with SAXS results for the more concentrated lamellar phase, while a headgroup thickness of 16 Å is consistent with an almost fully extended AA_5 chain. The SANS spectra indicate either isolated (unbound) bilayer fragments or unilamellar vesicles dispersed in aqueous solution. Polarizing optical microscopy of this sample shows the presence of maltese crosses, which indicates unilamellar vesicles are dispersed in aqueous solution. From the lowest accessible q of the SANS spectra, it can be inferred that the unilamellar vesicles are greater than 2000 Å in diameter.

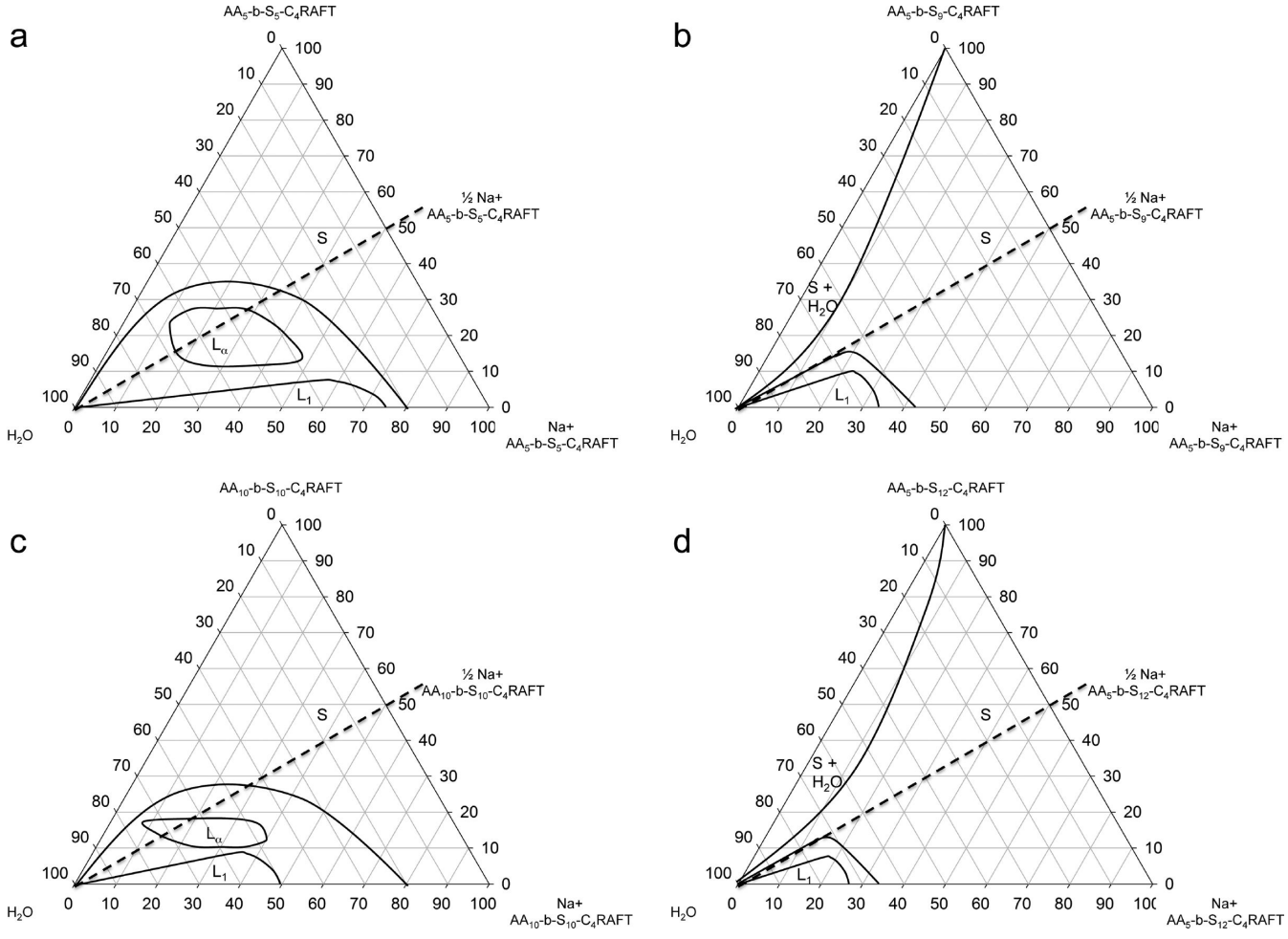

Figure 10. Ternary phase diagrams of (a) AA_5-b-S_5-C_4RAFT, (b) AA_5-b-S_9-C_4RAFT, (c) AA_{10}-b-S_{10}-C_4RAFT, and (d) AA_5-b-S_{12}−C4RAFT in water at 25 °C as a function of degree of ionization. The phase boundaries of the one-phase regions are drawn with a solid line. S, Lα, and L_1 denote solid, lamellar, and micellar phases. Concentrations are expressed in wt %.

dx.doi.org/10.1021/jp307875z | J. Phys. Chem. B 2013, 117, 3005−3018

AA_5-b-S_y-C_4RAFT. Figure 10 shows the ternary phase diagrams for AA_5-b-S_5-C_4RAFT, AA_5-b-S_9-C_4RAFT, AA_5-b-S_{12}-C_4RAFT, and AA_{10}-b-S_{10}-C_4RAFT in water as a function of AA block ionization. Like the AA_5-b-$BA_{n=5,9,12}$-C_4RAFT co-oligomer amphiphiles, the acidic forms of all styrene co-oligomers examined were insoluble in water. At 100% ionization, these co-oligomers became water-soluble and formed only an L_1 micellar phase. As noted above for the lamellar phase of AA_5-b-BA_y-C_4RAFT co-oligomers, the solubility limit of the L_1 phase is extremely sensitive to the hydrophobic to hydrophilic volume ratio. Lamellar nanostructures were the only liquid crystal phases formed by any of the $AA_{x=5,10}$-b-S_y-C_4RAFT diblock co-oligomers examined, and then only when the headgroup is partially ionized, and the degree of polymerization of the hydrophilic and hydrophobic blocks are equal.

SAXS spectra from the lamellar phase of $^1/_2Na^+$ AA_5-b-S_5-C_4RAFT are shown in Figure 11, and best-fit structural parameters from the head−tail lamellar bilayer model are summarized in Table 6. In contrast to the lamellar bilayers formed by the AA_5-b-BA_y-C_4RAFT co-oligomers, the headgroup and tail thickness of the $^1/_2Na^+$ AA_5-b-S_5-C_4RAFT membranes remain approximately constant upon dilution with water, and the bilayer spacing increases only slightly. As with the AA_5-b-BA_y-C_4RAFT co-oligomers, the S chains are contracted, which indicates the tails are intercalated with the tails of the opposing membrane. The Caillé parameter increases significantly upon dilution with water, and these $^1/_2Na^+$ AA_5-b-S_5-C_4RAFT membranes are more flexible than the corresponding $^1/_2Na^+$ AA_5-b-BA_5-C_4RAFT membranes.

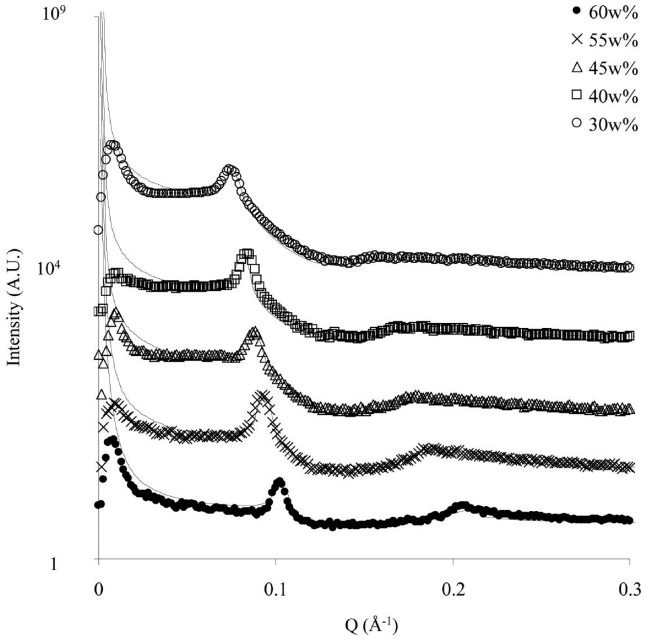

Figure 11. SAXS spectra of $^1/_2Na^+$ AA_5-b-S_5-C_4RAFT at 25 °C. Solid lines are fits to the head−tail lamellar model described in the text. Spectra have been offset by 10 for clarity.

Table 6. Summary of Nanostructures Formed by $^1/_2Na^+$ AA_5-b-S_5-C_4RAFT Determined by Best Fits of SAXS Data to the Head−Tail Lamellar Model Described in the Text

$^1/_2Na^+$ AA_5-b-S_5-C_4RAFT	headgroup thickness (Å)	tail thickness (Å)	lamellar spacing (Å)	H_2O:AA_5	Caillé
60 wt %	11	10	61	11.8	0.17
55 wt %	11	10	67	11.5	0.17
45 wt %	10	11	71	6.50	0.35
40 wt %	10	11	77	6.50	0.38
30 wt %	11	12	82	6.71	0.55

As observed for the Na^+ AA_5-BA_5-C_4RAFT, the SANS spectra of 1 wt % Na^+ AA_5-b-S_5-C_4RAFT are well-described by a core−shell spherical model. The core radius (11 Å) is nearly identical to the core radius of Na^+ AA_5-b-BA_5-C_4RAFT (13 Å) and yields the same aggregation number of 7. However, the shell thickness is smaller (12 Å, as opposed to 19 Å), which may be due to the lower aqueous solubility of styrene requiring increased shielding from the aqueous domain, and hence less solvation of the AA block.

CONCLUSIONS

The self-assembly of low molecular weight, amphiphilic block co-oligomers in aqueous solutions yields a rich structural polymorphism comparable to conventional small-molecule surfactants, and is dictated by both inter- and intramolecular interactions that depend on the composition and concentration of the polymers, as well as degree of ionization of the headgroup. The thermodynamically favorable self-assembled nanostructures of nonionic diblock co-oligomers correspond well to predictions based upon the hydrophobic to hydrophilic molecular volume ratio as a packing constraint. However, the excluded volume of ionic hydrophilic head groups is a strong function of the electrostatic repulsions, and is underestimated by a simple prediction of molecular volume based upon monomer density and molecular weight. Therefore, the ionic diblock co-oligomers tend to form structures with a higher than predicted curvature.

ASSOCIATED CONTENT

Supporting Information

A small-angle X-ray scattering spectrum of 25.0 wt % HEA_5-C_{12}RAFT with best fits to polydisperse core-*N* shell models, where $N = 1$, 2, and 3, and a polydisperse prolate ellipsoid model. This material is available free of charge via the Internet at http://pubs.acs.org.

AUTHOR INFORMATION

Corresponding Author

*E-mail: gregory.warr@sydney.edu.au.

Notes

The authors declare no competing financial interest.

ACKNOWLEDGMENTS

The authors acknowledge financial support from the Australian Research Council's Discovery Project, Linkage Project, and LIEF Schemes and from Dulux Australia and thank Algi Serelis of DuluxGroup for providing the RAFT agents used. This work utilized facilities supported in part by the National Science Foundation under Agreement No. DMR-0944772. We acknowledge the support of the National Institute of Standards and Technology, U.S. Department of Commerce, in providing the neutron research facilities used in this work, the ANSTO Bragg Institute for use of their Bruker NanoStar SAXS camera, and travel funding from the Access to Major Research Facilities Program.

REFERENCES

(1) Laughlin, R. *The Aqueous Phase Behavior of Surfactants*; Academic Press Limited: San Diego, CA, 1994.

(2) Israelachvili, J.; Michell, D.; Ninham, B. Theory of Self-Assembly of Hydrocarbon Amphiphiles into Micelles and Bilayers. *J. Chem. Soc., Faraday Trans. 2* **1976**, *72*, 1525−1568.

(3) Chiefari, J.; Chong, Y.; Ercole, F.; Krstina, J.; Le, T.; Mayadunne, R.; et al. Living Free-Radical Polymerization by Reversible Addition-Fragmentation Chain Transfer: The RAFT Process. *Macromolecules* **1998**, *31*, 5559−5562.

(4) Wang, J.; Matyjaszewski, K. Controlled Living Radical Polymerization-Halogen Atom-Transfer Radical Polymerization Promoted by a Cu(I)Cu(II) Redox Process. *Macromolecules* **1995**, *28*, 7901−7910.

(5) Chong, Y.; Le, T.; Moad, G.; Rizzardo, E.; Thang, S. A More Versatile Route to Block Copolymers and Other Polymers of Complex Architecture by Living Radical Polymerization. *Macromolecules* **1999**, *32*, 2071−2074.

(6) Coca, S.; Paik, H.; Matyjaszewski, K. Block Copolymers by Transformations of Living Ring-Opening Metathesis Polymerization Controlled/"Living" Atom Transfer Radical Polymerization. *Macromolecules* **1997**, *30*, 6513−6516.

(7) Kajiwara, A.; Matyjaszewski, K. Formation of Block Copolymers by Tranformation of Cationic Ring-Opening Polymerization to Atom Transfer Radical Polymerization (ATRP). *Macromolecules* **1998**, *31*, 3489−3493.

(8) Matsen, M.; Bates, F. Unifying Weak- and Strong-Segregation Block Copolymer Theories. *Macromolecules* **1996**, *29*, 1091−1098.

(9) Jain, S.; Bates, F. On the Origins of Morphological Complexity in Block Copolymer Surfactants. *Science* **2003**, *300*, 460−464.

(10) Alexandridis, P.; Olsson, U.; Lindman, B. A Record Nine Different Phases (Four Cubic, Two Hexagonal, and One Lamellar Lyotropic Liquid Crystalline and Two Micellar Solutions) in a Ternary Isothermal System of an Amphiphilic Block Copolymer and Selective Solvents (Water and Oil). *Langmuir* **1998**, *14*, 2627−2638.

(11) Bates, F.; Fredrickson, G. Block Copolymer Thermodynamics: Theory and Experiment. *Annu. Rev. Phys. Chem.* **1990**, *41*, 525−557.

(12) Ikkala, O.; ten Brinke, G. Hierarchical Self-Assembly in Polymeric Complexes: Towards Functional Materials. *Chem. Commun.* **2004**, *19*, 2131−2137.

(13) Alexandridis, P. Amphiphilic Copolymers and Their Applications. *Curr. Opin. Colloid Interface Sci.* **1996**, *1*, 490−501.

(14) Holder, S.; Sommerdijk, N. New Micellar Morphologies from Amphiphilic Block Copolymers: Disks, Toroids, and Biocontinuous Micelles. *Polym. Chem.* **2011**, *2*, 1018−1028.

(15) O'Reilly, R.; Hawker, C.; Wooley, K. Cross-Linked Block Copolymer Micelles: Functional Nanostructures of Great Potential and Versatility. *Chem. Soc. Rev.* **2006**, *35*, 1068−1083.

(16) Reynhout, I.; Cornelissen, J.; Nolte, R. Synthesis of Polymer-Biohybrids: From Small to Giant Surfactants. *Acc. Chem. Res.* **2009**, *42*, 681−692.

(17) Borisov, O.; Zhulina, E.; Leermakers, F.; Muller, A. Self-Assembled Structures of Amphiphilic Block Copolymers: Theory, Self-Consistent Field Modeling and Experiment. *Adv. Polym. Sci.* **2011**, *241*, 57−129.

(18) Choucair, A.; Eisenberg, A. Control of Amphiphilic Block Copolymer Morphologies Using Solution Conditions. *Eur. Phys. J. E* **2003**, *10*, 37−44.

(19) Termonia, Y. Sphere-to-Cylinder Transition in Dilute Solutions of Diblock Copolymers. *J. Polym. Sci., Part B: Polym. Phys.* **2002**, *40*, 890−895.

(20) Panagiotopoulos, A.; Floriano, M.; Kumar, S. Micellization and Phase Separation of Diblock and Triblock Model Surfactants. *Langmuir* **2002**, *18*, 2940−2948.

(21) Siauw, M.; Hawkett, B. S.; Perrier, S. Short Chain Amphiphilic Diblock Co-Oligomers via RAFT Polymerization. *Polym. Chem.* **2012**, *50*, 187−198.

(22) Braun, J.; Bruns, N.; Pfohl, T.; Meier, W. Phase Behavior of Vesicle-Forming Block Copolymers in Aqueous Solutions. *Macromol. Chem. Phys.* **2011**, *212*, 1245−1254.

(23) Astafieva, I.; Khougaz, K.; Eisenberg, A. Micellization in Block Polyelectrolyte Solutions. 2. Fluorescence Study of the Critical Micelle Concentration as a Function of the Soluble Block Length and Salt Concentration. *Macromolecules* **1995**, *28*, 7127−7134.

(24) Astafieva, I.; Khougaz, K.; Eisenberg, A. Micellization in Block Polyelectrolyte Solutions. 3. Static Light Scattering Characterization. *Macromolecules* **1995**, *28*, 7135−7147.

(25) Astafieva, I.; Zhong, X.; Eisenberg, A. Critical Micellization Phenomena in Block Copolymer Electrolye Solutions. *Macromolecules* **1993**, *26*, 7339−7352.

(26) Shen, H.; Eisenberg, A. Block Length Dependence of Morphological Phase Diagrams of the Ternary System of PS-b-PAA/Dioxane/H_2O. *Macromolecules* **2000**, *33*, 2561−2572.

(27) Zhang, L.; Eisenberg, A. Multiple Morphologies of Crew-Cut Aggregates of Polystyrene-b-Poly(acrylic acid) Block-Copolymers. *Science* **2005**, *268*, 1728−1731.

(28) Colombani, O.; Ruppel, M.; Burkhardt, M.; Drechsler, M.; Schumacher, M.; Gradzielski, M.; et al. Structure of Micelles of Poly(n-butyl acrylate)-block-poly(acrylic acid) Diblock Copolymers in Aqueous Solution. *Macromolecules* **2007**, *40*, 4351−4362.

(29) Cristobal, G.; Berret, J.; Chevallier, C.; Talingting-Pabalan, R.; Joanicot, M.; Grillo, I. Phase Behavior of Polyelectrolyte Block Copolymers in Mixed Solvents. *Macromolecules* **2008**, *41*, 1872−1880.

(30) Jacquin, M.; Muller, P.; Talingtin-Pabalan, R.; Cottet, H.; Berret, J.; Futterer, T.; et al. Chemical Analysis and Aqueous Solution Properties of Charged Amphiphilic Block Copolymers PBA-b-PAA Synthesized by MADIX. *J. Colloid Interface Sci.* **2007**, *316*, 897−911.

(31) Demus, D.; Richter, L. *Textures of Liquid Crystals*, 2nd ed.; Verlag Chemie: New York, 1980.

(32) Hyde, S. Identification of lyotropic liquid crystalline mesophases. In *Handbook of Applied Surface and Colloid Chemistry*; Holmberg, K., Ed.; John Wiley & Sons: New York, 2002; Vols. *1*−*2*, pp 299−327.

(33) Rosevear, F. Liquid Crystals-Mesomorphic Phases of Surfactant Compositions. *J. Soc. Cosmet. Chem.* **1968**, *19*, 581−594.

(34) Rosevear, F. The Microscopy of the Liquid Crystalline Neat and Middle Phases of Soaps and Synthetic Detergents. *J. Am. Oil Chem. Soc.* **1954**, *31*, 628−639.

(35) Saupe, A. Textures, Deformations, and Structural Order of Liquid-Crystals. *J. Colloid Interface Sci.* **1977**, *58*, 549−558.

(36) Kline, S. Reduction and Analysis of SANS and USANS Data Using IGOR Pro. *J. Appl. Crystallogr.* **2006**, *39*, 895.

(37) Bartlett, P.; Ottewill, R. A Neutron-Scattering Study of the Structure of a Bimodal Colloidal Crystal. *J. Chem. Phys.* **1992**, *96*, 3306−3318.

(38) Nallet, F.; Laversanne, R.; Roux, D. Modeling X-ray or Neutron-Scattering Spectra of Lyotropic Lamellar Phases-Interplay Between Form and Structure Factors. *J. Phys. II* **1993**, *3*, 487−502.

(39) Fontell, K.; Ceglie, A.; Lindman, B.; Ninham, B. Some Observations on Phase-Diagrams and Structure in Binary and Ternary-Systems of Didodecyldimethylammonium Bromide. *Acta Chem. Scand., Ser. A* **1986**, *40*, 247−256.

(40) Patrick, H. N.; Warr, G. G. Counterion Binding and Regulation of Interfaces Between Charged Bilayers. *J. Phys. Chem.* **1996**, *100*, 16268−16274.

(41) Hishida, M.; Seto, H. Lamellar-Lamellar Phase Separation of Phospholipid Bilayers Induced by Salting-in/-out Effects. *J. Phys.: Conf. Ser.* **2011**, *272*, 1−6.

(42) Dubois, M. Z. Swelling Limits for Bilayer Microstructures: the Implosion of Lamellar Structure versus Disordered Lamellae. *Curr. Opin. Colloid Interface Sci.* **2000**, *5*, 27−37.

(43) Wennerstrom, H. The Unbinding Transition and Lamellar Phase Lamellar Phase Coexistence. *Langmuir* **1990**, *6* (4), 834−838.

(44) Deme, B.; Dubois, M.; Zemb, T.; Cabane, B. Coexistence of Two Lyotropic Lamellar Phases Induced by a Polymer in a Phospholipid-Water System. *Colloids Surf., A* **1997**, *121*, 135−143.

(45) Skouri, M.; Marignan, J.; May, R. X-ray and Neutron-Scattering Study of the Lamellar and L3-Phases of the System Aerosol-OT-Water-Effect of NaCl and Decane. *Colloid Polym. Sci.* **1991**, *269*, 929−937.

(46) Ho, D.; Briber, R.; Glinka, C. Characterization of Organically Modified Clays Using Scattering and Microscopy Techniques. *Chem. Mater.* **2001**, *13*, 1923−1931.
(47) Ganeva, D.; Sprong, E.; de Bruyn, H. W.; Warr, G. G.; Such, C.; Hawkett, B. Particle Formation in Ab Initio RAFT Mediated Emulsion Polymerization Systems. *Macromolecules* **2007**, *40*, 6181−6189.
(48) Kotlarchyk, M.; Chen, S. Analysis of Small-Angle Neutron Scattering Spectra from Polydisperse Interacting Colloids. *J. Chem. Phys.* **1983**, *79*, 2461−2469.
(49) Berr, S. Solvent Isotope Effects on Alkyltrimethylammonium Bromide Micelles as a Function of Alkyl Chain-Length. *J. Phys. Chem.* **1987**, *91*, 4760−4765.